How does prestrain in the tympanic membrane affect middle-ear function? A finite-element model study in rabbit

# How does prestrain in the tympanic membrane affect middle-ear function? A finite-element model study in rabbit

Pieter G.G. Muyshondt[a,1], Joris J.J. Dirckx[a]

[a] *University of Antwerp, Biophysics and Biomedical Physics, Groenenborgerlaan 171, B-2020 Antwerp, Belgium*

[1] Corresponding author; *E-mail:* pieter.muyshondt@uantwerpen.be

## Abstract

Experiments have shown that prestrain exists in the rabbit tympanic membrane (TM), also in the absence of external loads. To date, it is unclear how prestrain influences the vibration response of the middle ear (ME). In this study, a detailed 3D finite-element model of the rabbit ME was constructed based on experimentally validated material properties. The model incorporates different degrees of prestrain in the TM and simulates the ME vibration response to sound as a linear harmonic perturbation around the prestressed reference state. To account for finite deformations associated with large prestrains, a framework was developed that iteratively updates the initial unstrained geometry until the prestrained geometry is in agreement with the given reference geometry. After validating the model using quasi-static and acoustic measurement data, it was shown that small levels of prestrain already have a substantial impact on the normal umbo and footplate response due to a phenomenon known as prestress stiffening. Although the approach is not preferable, it was possible to replicate the effect of prestrain in the normal ME by appropriately scaling the elastic moduli and damping factors in the base model. To evaluate the effect of possible changes in TM prestrain when the normal state of the ear is altered due to pathological modifications in the ME structure, we created a model with a perforation in the TM. It was shown that the change in vibration response after perforation is affected at low frequencies by a release of TM prestrain. In future studies, it may be necessary to incorporate prestrain in ME models to better understand the function of the diseased or reconstructed ME, which may be relevant for the development of reconstructive tissue grafts in the middle ear.

## Keywords

finite-element analysis; prestrain; rabbit; tympanic membrane; middle ear

## Glossary

AMP, anterior mallear process; CT, computed tomography; FE, finite element; IM, incudomalleolar; IS, incudostapedial; ME, middle ear; PF, pars flaccida; PIL; posterior incudal ligament; PT, pars tensa; SAL, stapes annular ligament; TM, tympanic membrane

## 1. Introduction

Experiments on biological structures have revealed that tissues like membranes, ligaments, muscles and tendons retract after they are cut out of the body. This retraction is a result of *strains* and *stresses* that exist in the normal state of the body, which are partially released when the tissue is excised. Strain describes the extension or compression of a material with respect to a certain reference state, whereas stress describes the associated internal force that arises in the body to reach equilibrium. When a material holds strain and stress in its rest state in the absence of external loads, we speak of prestrain and prestress, often also referred to as resting or *in-situ* strain and stress. Prestrain and prestress occur in many biological structures and are believed to originate from the growth and remodeling of tissue (Ambrosi et al., 2011).

Up till now it has not been entirely clear whether prestrain exists in the mature eardrum or tympanic membrane (TM). The TM is a curved and conical membrane that is composed of three layers: an outer epidermis layer, an inner mucosal layer, and a middle layer called the lamina propria, which is built up of two families of radially and circumferentially oriented collagen fibers embedded in connective tissue (Filogamo, 1949). To detect prestrain in the TM of humans and other mammals, von Békésy (1949) and Kirikae (1960) created incisions in the membrane and observed if the tissue showed any retraction. However, the results were not conclusive about the existence and nature of the prestrain, because the prestrain may be too small to be detected with early techniques based on pure visual observation (Funnell and Laszlo, 1982). With the advent of new sensitive measurement techniques, it has become possible to resolve microscopic changes in strain, which enables the detection of prestrain and prestress in biological structures (Nelson, 2013, 2014). Recently, we have performed experiments on fresh cadaveric rabbit ears, in which the change of the strain in the TM was measured by digital image correlation after creating radial and circumferential incisions in the membrane (Livens et al., 2021). The experiments indicate the existence of a certain degree of prestrain in the TM, with no clear differences between radial and circular cuts and between the different locations on the membrane.

With the existence of prestrain and prestress in the TM, the question arises how they influence the mechanical response of the ME to sound pressure loading. Preliminary model simulations that incorporate TM prestrain in the human ME have revealed a clear shift in the modal frequencies of the membrane for small prestrain levels of up to 1% (Caminos et al., 2018). In the locust, it has been shown that TM prestrain is needed to explain the propagation of flexural waves and the localization of kinetic energy on the membrane (Malkin et al., 2014). So far, it has been unclear how prestrain and prestress in the TM relates to possible prestrain and prestress in other parts of the ME, which should be in equilibrium in the reference configuration of the geometry. It has been suggested that there are

preloads in the suspensory ligaments of the ossicles to balance the preloads in the TM that pull the membrane outwards (Sim and Puria, 2008). Alternatively, the ossicles and ligaments may change their orientation during growth, pulling the TM inwards (Marcusohn and Dirckx, 2011). However, it is unclear if strain is developed in the TM this way, and if so, whether it is maintained during adulthood. Nevertheless, the observation that the TM loses its original shape when the suspensory ligaments are cut (Dirckx and Decraemer, 2001) or when the manubrium is fractured (Gladiné et al., 2018) suggest the existence of at least some form of (a release in) prestrain and prestress.

In the present paper, we investigate the effect of prestrain in the TM on the vibration response of the ME in rabbit by means of finite-element (FE) modeling. The prestrain in the TM as measured in experiments is incorporated in a 3D FE model of the entire ME based on detailed micro-tomography data. The material parameters of the different components in the model are based on experimental data of the material properties. Prestrain is incorporated by radially stretching the outer rim of the membrane. To include large finite prestrains in the reference geometry of the ME, a framework is developed that iteratively updates the unstrained geometry of the ME model until the deformed prestrained geometry is in agreement with the original reference geometry. After the model is successively prestrained, the frequency response is computed as a linear perturbation around the prestressed state. After validating the model to experimental data, we investigate the effect of different levels of prestrain on the ME response for both the normal ear and pathological modifications to the normal structural condition. A sensitivity analysis is done to evaluate the influence of the different model parameters.

## 2. Materials and methods

### *2.1. Model geometry*

The FE model is based on the right ear of a New-Zealand white rabbit, scanned with micro-CT at the Center of X-Ray Tomography of Ghent University (Masschaele et al., 2013). The sample was stained with iodine ($I_2$) to enhance soft-tissue contrast. The voxel pitch of the reconstructed 3D tomographic scan was 9 µm. Semi-automatic image segmentation tools were used in Amira 6.3.0 (FEI, Hillsboro, OR, USA) to identify the different ME components. The obtained segmented 3D data set was converted to a surface model composed of triangular elements. The final model includes the malleus, incus and stapes, the pars tensa (PT), the pars flaccida (PF), the incudomalleolar (IM) joint, the incudostapedial (IS) joint, the posterior incudal ligament (PIL), the stapes annular ligament (SAL) and the anterior mallear process (AMP). As in the gerbil ME model of Maftoon et al. (2015), the tensor tympani was excluded from the model. Severing this muscle was shown to have no effect on ME deformations (Dirckx and Decraemer, 2001). Neither the stapedial muscle tendon was included in the model:

because the current study does not investigate the effect of active contraction of the tensor tympani and tensor stapedius, including these components is neither relevant in this regard. Also smaller ligaments visible in the scan, such as the lateral mallear ligament and the superior incudal ligament, were excluded from the model. The final model geometry is shown in Fig. 1.

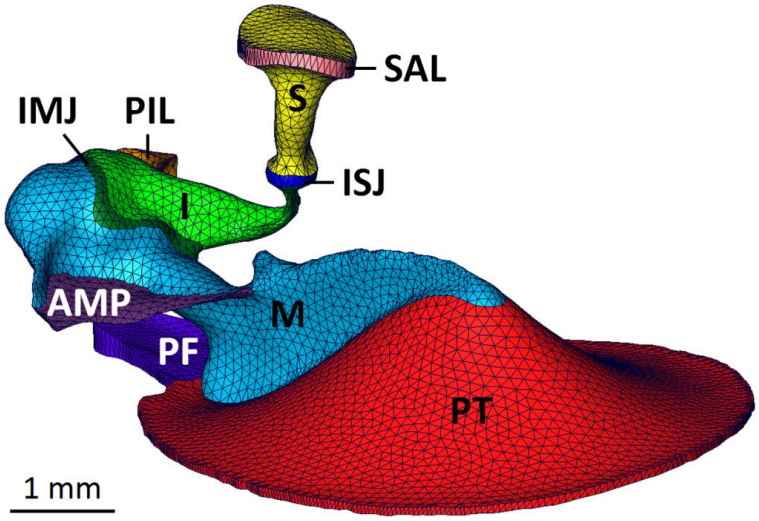


**Fig. 1.** 3D surface model of the rabbit middle ear with the different components indicated. PT, pars tensa; PF, pars flaccida; M, malleus; I, incus; S, stapes; AMP, anterior mallear process; PIL, posterior incudal ligament; IMJ, incudomalleolar joint; ISJ, incudostapedial joint; SAL, stapes annular ligament.

The PT and SAL in the segmented data set are thin compared to the other structures, so their thickness distributions determined from the micro-CT scan have a lower relative precision than the other components. The segmented model of the PT has a thickness of about 25 µm in the major part of the membrane's body, which is in agreement with histology measurements of the PT thickness in rabbit (Chole and Kodama, 1989). Close to the outer rim of the PT and the connection with the PF, the PT thickness increases considerably up to 80 µm. The thickness of the SAL around the stapes footplate comprises only about a single voxel in the scan. Due to a lack of more precise measurements of the SAL in rabbit, a constant thickness equal to the scan resolution of 9 µm was assigned to the ligament in the final surface model.

The geometrical surface model was exported to the commercial FE software COMSOL Multiphysics 6.0 (COMSOL Inc, Burlington, MA, USA), extended with the Structural Mechanics Module, the Nonlinear Structural Materials Module, and the LiveLink with MATLAB. The triangular surface model was converted to a volumetric mesh of second-order solid elements. The PT and PF were modeled as prism elements, with the quadrilateral faces oriented parallel to the mediolateral axis. All other structures were modeled as tetrahedral elements. A single layer of prism elements was considered through the thickness of the TM, because doubling the number of layers had only a minor effect on the output for all frequencies (< 0.2 dB).

## 2.2. *Material properties*

Although the deformations associated with sound-induced ME biomechanics can be considered as infinitesimal for moderate to high sound pressures levels (< 120 dB), the deformations induced by moderate to high prestrains cannot. For this reason, it was necessary to use finite deformation theory and describe the nonlinear stress-strain response of the ME soft-tissue structures by hyperelastic material characterizations. Hyperelastic models for nonlinear elastic materials are defined by a strain-energy function $W$, which is typically split into an isochoric part $W_{\mathrm{iso}}$ and a volumetric part $W_{\mathrm{vol}}$ for isotropic and nearly incompressible materials (e.g., Cescotto and Fonder, 1979):

$$W = W_{\mathrm{iso}}(\bar{I}_1, \bar{I}_2) + W_{\mathrm{vol}}(J). \tag{1}$$

In this equation, we have the volume ratio $J = \sqrt{\det(\mathbf{C})} = \lambda_1\lambda_2\lambda_3$, where $\lambda_i$ are the three principal stretches of the material ($i = 1,2,3$) and $\mathbf{C}$ is the right Cauchy-Green deformation tensor given by $\mathbf{C} = \mathbf{F}^{\mathrm{T}}\mathbf{F}$. The tensor $\mathbf{F} = \partial\mathbf{x}/\partial\mathbf{X}$ is the deformation gradient, with $\mathbf{x}$ and $\mathbf{X}$ the coordinate vectors in the deformed and undeformed configuration of the material, respectively. In Eq. (1), $\bar{I}_1 = J^{-2/3}I_1$ and $\bar{I}_2 = J^{-4/3}I_2$, with $I_1 = \mathrm{tr}(\mathbf{C}) = \lambda_1^2 + \lambda_2^2 + \lambda_3^2$ the first invariant of $\mathbf{C}$ and $I_2 = [\mathrm{tr}(\mathbf{C})^2 - \mathrm{tr}(\mathbf{C}^2)]/2 = \lambda_1^2\lambda_2^2 + \lambda_2^2\lambda_3^2 + \lambda_3^2\lambda_1^2$ the second invariant of $\mathbf{C}$.

To simulate in-plane prestrain and prestress in the TM, we need material data of the in-plane stress-strain response of the PT over a sufficiently broad strain range. Such data was collected most recently in uniaxial tensile tests on the human PT by Cheng et al. (2007). Because their measurements were performed on cut-out PT strips, any possible effect of *in-situ* TM prestrain in the native ME on the determined elastic parameters was eliminated. To create a hyperelastic model of the PT, we fitted an isotropic Veronda-Westmann model to their stress-strain data as it was analyzed in Motallebzadeh et al. (2013). More details on how this was done can be found in our nonlinear model of the human ME (Muyshondt and Dirckx, 2021). The isochoric strain-energy density $W_{\mathrm{iso}}$ of a Veronda-Westmann model is given by

$$W_{\mathrm{iso}} = \mu\left[\frac{\mathrm{e}^{b(\bar{I}_1-3)} - 1}{b} - \frac{\bar{I}_2 - 3}{2}\right]. \tag{2}$$

with $\mu$ the shear modulus of the material in the limit of zero strain (or $\lambda_i = 1$), and $b$ a parameter describing the change of stress with the strain in the material. Due to the specific collagen fiber arrangement of the PT, it has been claimed that the elasticity of the PT is anisotropic, having different elastic moduli in the radial, circumferential and transversal direction. For the sake of simplicity, and because O'Connor et al. (2017) found that a model with

isotropic PT Young's modulus was able to approximate the ME frequency response largely as well as a PT model with anisotropic elastic moduli, we decided to use an isotropic elastic model for the PT.

To determine the nonlinear elastic parameters of the other soft-tissue structures, we applied the same fitting procedure as for the PT when experimental stress-strain data was available in the literature. This was the case for the SAL (Gan et al., 2011) and the ISJ (Zhang and Gan, 2011). For the IMJ no such data exists, so we used the same Veronda-Westmann parameters as for the ISJ. Also for the PIL no such data is available; to describe the elasticity of this component we used a Neo-Hookean solid, which is defined as

$$W_{\text{iso}} = \frac{\mu}{2}(\bar{I}_1 - 3), \tag{3}$$

with $\mu$ the shear modulus. Different values have been used for the elastic modulus of the PIL, with shear moduli ranging from 0.05 MPa (Zhang et al., 2020) to 21.6 MPa (i.e. a Young's modulus of 65 MPa in case of incompressibility; Tian et al., 2015). We used a shear modulus of 10 MPa to obtain a good agreement with measurements of quasi-static and vibroacoustic ME motion (see Results section). The PF, which is a continuation of the ear-canal skin (Lim, 1968), is typically considered to have a lower elasticity than the PT. We simulated the PF as a Neo-Hookean material with a shear modulus of 1/10th of the PT.

To simulate near incompressibility of the soft tissues, a volumetric strain-energy density defined by

$$W_{\text{vol}} = \frac{K}{2}(J - 1)^2 \tag{4}$$

was used, with $K$ the bulk modulus of the material. For each soft-tissue component, $K$ was assumed to be a 100 times higher than $\mu$, corresponding to a Poisson's ratio $\nu$ of 0.495. The bony malleus, incus and stapes were modeled as linear elastic materials using a Young's modulus $E$ of 16 GPa as measured by Soons et al. (2010) in rabbit, with $\nu = 0.3$. The anterior mallear process in rabbit is also made of bone (Dirckx and Decraemer, 2001), so we used the same elastic parameters as for the ossicles.

The mass densities of the bony structures in the model were taken from values reported by Buytaert et al. (2011) in gerbil, which were equal to 1740 kg/m$^3$ for the malleus, incus and anterior mallear process, and 1370 kg/m$^3$ for the stapes. The mass density of the soft-tissue components was chosen equal to 1100 kg/m$^3$, which holds the middle between pure collagen (1200 kg/m$^3$) and water (1000 kg/m$^3$). To take into account damping in the harmonic response of the ME, a constant loss factor of 0.1 was assigned to all soft-tissue structures, as was done in De Greef et al. (2017) for the TM. All materials parameters are summarized in Table 1.

| Nearly incompressible Veronda–Westmann materials | | | | | |
|---|---|---|---|---|---|
| *Component* | $\mu$ (MPa) | $b$ | $K$ (MPa) | $\rho$ (kg/m$^3$) | $\eta$ |
| PT | 0.5 | 22.02 | 50 | 1100 | 0.1 |
| SAL | $9.72 \cdot 10^{-3}$ | 0.214 | 0.972 | 1100 | 0.1 |
| ISJ | 0.142 | 1.47 | 14.2 | 1100 | 0.1 |
| IMJ | 0.142 | 1.47 | 14.2 | 1100 | 0.1 |
| **Nearly incompressible Neo-Hookean materials** | | | | | |
| *Component* | $\mu$ (MPa) | | $K$ (MPa) | $\rho$ (kg/m$^3$) | $\eta$ |
| PIL | 10 | | 1000 | 1100 | 0.1 |
| PF | 0.05 | | 5 | 1100 | 0.1 |
| **Linear elastic materials** | | | | | |
| *Component* | $E$ (MPa) | | $\nu$ | $\rho$ (kg/m$^3$) | $\eta$ |
| Malleus | $16 \cdot 10^3$ | | 0.3 | 1740 | 0 |
| AMP | $16 \cdot 10^3$ | | 0.3 | 1740 | 0 |
| Incus | $16 \cdot 10^3$ | | 0.3 | 1740 | 0 |
| Stapes | $16 \cdot 10^3$ | | 0.3 | 1370 | 0 |

**Table 1.** Material parameters of the base model. For the PT, SAL and ISJ, we calculated $\mu$ and $b$ by fitting a Veronda-Westmann model to the stress-strain response of the Ogden model in Motallebzadeh et al. (2013), Gan et al. (2011) and Zhang and Gan (2011), respectively. $\mu$, shear modulus; $b$, second Veronda-Westmann parameter; $K$, bulk modulus; $\nu$, Poisson's ratio; $\rho$, mass density; $\eta$, loss factor.

### *2.3. Modeling procedure*

The modeling procedure was split up in two steps: in the first step, a method was used to generate stationary prestrains in the PT of different magnitudes; in the second step, the output of the first model step was used as initial condition to compute the long-term static and linear harmonic response of the ME to pressure loading at the level of the TM.

#### *2.3.1. Prestrain step*

In our measurements of TM prestrain in rabbit, we found no clear difference in the strain values between the radial and circumferential direction and between different locations (Livens et al., 2021). When a flat circular membrane is radially stretched at the rim, the strain in the membrane will be homogeneous and equal in the radial and the circumferential direction. Therefore, to generate prestrain in the PT in our model, the PT was stretched at the rim by prescribing a radial displacement that equals a fixed percentage of the radial distance to the umbo (0.5%, 1%, 2%, 4% and 8%). This range was roughly based on the mean and standard deviation of the average prestrain values at the different TM locations reported in Livens et al. (2021), which were derived from the maximal

prestrain values measured at the incisions. Near the connection with the PF, the prescribed displacement of the PT rim was gradually forced to zero to avoid prestraining of the PF.

The prestrain in the TM is present in the reference geometry of the ME as imaged by the micro-CT scan. Our method to generate TM prestrain, however, causes a distortion of the ME geometry, which may be substantial for even moderate degrees of prestrain, hence affecting the model outcome. To make the prestrain compatible with the reference geometry, we created a method that iteratively updates the coordinates of the undeformed input geometry which, after successful prestraining, leads to a deformed geometry that is in agreement with the original reference geometry. If the coordinates of the model are denoted by $\boldsymbol{X}_0$ for the original undeformed reference geometry, $\boldsymbol{X}_i$ for the undeformed geometry at iteration $i$, and $\boldsymbol{x}_i$ for the deformed geometry at iteration $i$, then the coordinates of the undeformed geometry at the subsequent iteration $\boldsymbol{X}_{i+1}$ are calculated by $\boldsymbol{X}_{i+1} = \boldsymbol{X}_0 - (\boldsymbol{x}_i - \boldsymbol{X}_i)$. Starting at $\boldsymbol{X}_1 = \boldsymbol{X}_0$, the iterative process is continued until the maximal error of all vertices between the prestrained geometry and the original reference geometry $\|\boldsymbol{x}_i - \boldsymbol{X}_0\|_2$ is considered small enough, with $\|\cdot\|_2$ the Euclidean norm. The updating routine was automated in MATLAB through the COMSOL LiveLink.

As suggested in previous studies, the prestress associated with prestrain in the TM may be balanced with the prestress in other parts of the ME. To account for this effect in the prestrain calculation step, we constrained the SAL, PIL and AMP by fixing the displacement degrees of freedom at their connection to the ME cavity walls. As the PT is deformed during the prestrain calculation step, the other ME components are able to deform in conjunction with the PT. By fixing these components at the walls, they have the ability to develop a certain degree of prestress to reach equilibrium with the prestress in the PT.

### *2.3.2. Pressure loading step*

After the model was successfully prestrained by stretching the rim of the PT, the PT rim was held fixed and a static or harmonic pressure load was applied to the lateral TM surface to compute either the long-term static or harmonic response of the ME. The long-term response of the ME to static pressure at the TM was computed for pressures up to +2 and −2 kPa, taking into account nonlinearity of the deformation. The harmonic response of the ME to sound-pressure loading was simulated by applying a uniform harmonic pressure to the TM with frequencies between 0.5 and 8 kHz at 16 frequencies per octave and an amplitude of 1 Pa. Hence, the calculated vibration response was normalized with respect to input pressure. Because sound-induced ME motions can be considered linear for sound-pressure levels up to about 120 dB, the steady-state response was computed in the frequency domain as a linear perturbation around the prestressed step, as was done in Muyshondt and Dirckx (2021) to compute the effect of static pressure on harmonic ME vibrations.

To take into account the impedance load of the cochlea, a uniform pressure $p_C = z_C v_{FP}$ was imposed on the medial footplate surface, with $z_C$ the specific acoustic impedance of the cochlea and $v_{FP}$ the out-of-plane footplate velocity. According to Hemilä et al. (1995), $z_C$ is purely viscous and independent of animal size with a constant value of 140 kPa s/m for all frequencies, which was used in our model. With this assumption, the cochlear impedance will only affect the dynamic and not the static ME response, which is in agreement with the observation that removing the cochlea in rabbit has a negligible effect on quasi-static TM deformation (Dirckx and Decraemer, 2001). The load on the footplate $p_C$ was only defined in the out-of-plane direction, hence assuming that cochlear loads induced by footplate rocking motion are negligible. As in our most recent model of the human ME (Muyshondt and Dirckx, 2021), the acoustic impedances of the ear canal and the ME cavity were ignored.

### *2.3.3. Middle ear with structural changes*

Besides the fact that prestrain may affect the vibration response of the normal ME, it is also possible that structural changes in the ME due to a disease or surgical reconstruction will change the state of prestrain in the TM, hence influencing the change in ME response. For example, when the TM is perforated, the change in ME response may be affected by changes in TM prestrain due to the perforation. To test this hypothesis, we created an additional model with a 2-mm diameter hole in the posterior-inferior quadrant of TM by removing the elements of the perforation from the model geometry, and calculated the effect on the vibration response for a model with and without prestrain. The model outcome does not depend on whether the prestrain or the perforation is applied first; we first created the perforation and then incorporated prestrain, as this order is computationally more straightforward. Just like in the simulations of the normal ME, prestrain in the PT was induced by stretching the outer rim of the membrane. As a result, the boundaries of the applied perforation will deform accordingly to reach static equilibrium. After perforating and prestraining the TM, sound pressure loads were applied to the remaining portion of the lateral TM surface. Because the model does not include the ear canal and ME air spaces, the leakage of sound pressure across the hole is not taken into account, even though it was shown to have an important effect (Voss et al., 2001). Hence, our model can only be used to examine the effect of changes in prestrain on the vibration response upon perforation. In reality, a perforation will also balance possible static pressure gradients across the TM, but as we are studying the effect of prestrain in the absence of external loads this effect is not considered here.

## 3. Results

### *3.1. Prestrain analysis*

To evaluate the effect of different levels of prestrain in the TM, radial displacements of 0.5%, 1%, 2%, 4% and 8% of the distance to the umbo are imposed on the rim of the PT in the prestrain analysis step. The updating procedure of the model geometry described in Section 1.2.1 is continued until the difference between the coordinates of the prestrained geometry and the original reference geometry is smaller than 9 µm for all vertices, that is, smaller than the resolution of the micro-CT scan on which the ME model is based. For the largest prestrain value (8%), this condition is met after 12 iterations. The generated prestrain in the membrane's body is evaluated by calculating the average von Mises strain of the Green-Lagrange strain tensor, which is a positive scalar quantity that describes the state of strain in a material. The von Mises strain is equal to 0.52%, 1.02%, 1.99%, 3.83% and 7.48% for the 5 chosen prestrain states, which is in close agreement with the respective fractions of the radial displacements (0.5%, 1%, 2%, 4% and 8% of the distance to the umbo) prescribed at the PT rim to generate prestrain in the model. The von Mises stress of the second Piola-Kirchhoff stress tensor, describing the state of stress in the PT, is equal to 7.95, 15.5, 32.0, 73.2 and 244 kPa for the 5 prestrain states. Fig. 2 shows the von Mises strain in the PT together with the direction of the first principal strain (corresponding the most positive eigenvalue of the Green-Lagrange strain tensor) for the different prestrain levels. Fig. 2 reveals that the prestrain in the PT is oriented more circumferentially in the outer regions near the rim and more radially in the inner parts near the manubrium. Also, the von Mises strain field becomes more uniform as prestrain increases.

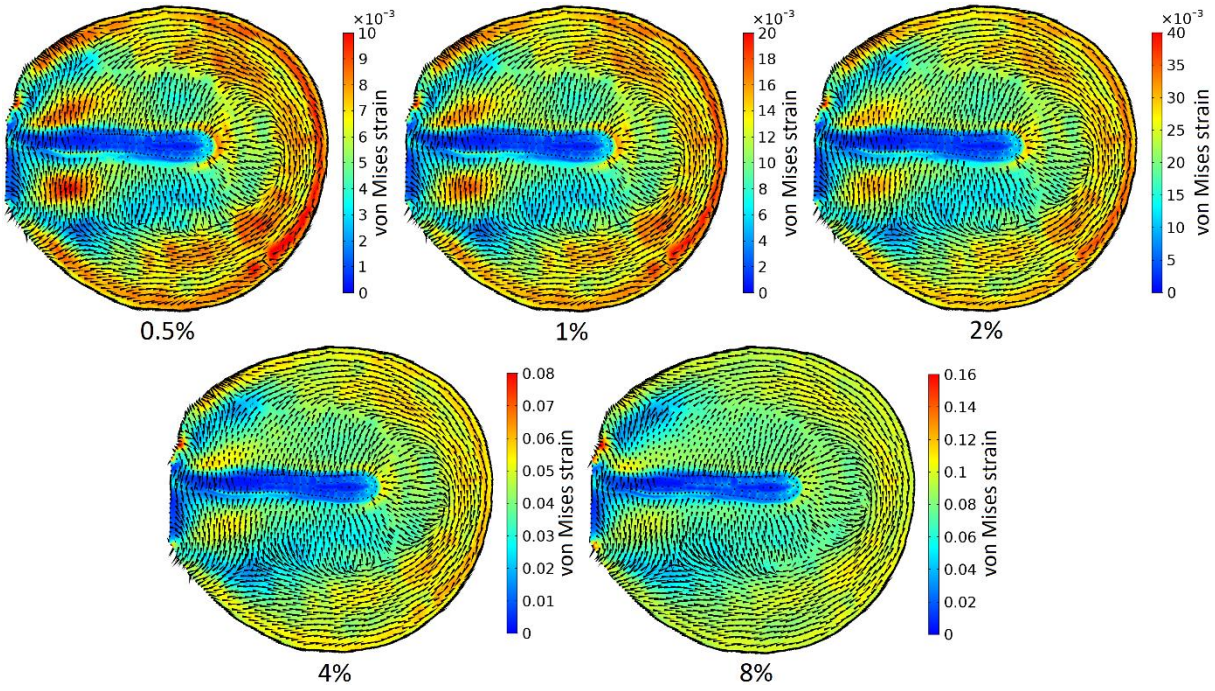


**Fig. 2.** Von Mises strain field in the pars tensa upon stretching the rim of the membrane by different prestrain values, including the direction of the first principal strain. The direction of the prestrain is more circumferential near the periphery and more radial near the manubrium.

### *3.2. Static response*

Before studying the effect of different degrees of TM prestrain on the harmonic ME response, we validate the static stress-strain response of the model by comparing it to quasi-static experiments of umbo motion, which were collected most recently in rabbit by Gladiné and Dirckx (2019). Digital image correlation was used to measure quasi-static TM deformation in response to triangular pressure cycles at the TM with a frequency of 0.03125 Hz and a peak pressure of 2 kPa. Because our model computes the long-term static response, time-dependent viscoelastic effects such as hysteresis observed in the experiments are not taken into account. Fig. 3 compares the umbo displacement as a function of input pressure at the TM for the experiment (a; mean and standard deviation) and the model for different degrees of prestrain (b). It is seen that the lateral displacement of the umbo under negative pressure is larger than the medial displacement under positive pressure in both the experiment and model. When the prestrain in the model is increased, it becomes clear that the asymmetry and nonlinearity of the displacement curve between positive and negative pressures diminishes. For prestrains of 4% and 8%, the change relative to the curve with 0% prestrain and the difference with the measurements becomes too high, so these prestrain values appear too extreme for the present base model. For smaller prestrains up to 2%, the change relative

to the 0% prestrain case is smaller than the variation between the measurements, and the model outcome is in line with the measurement results.

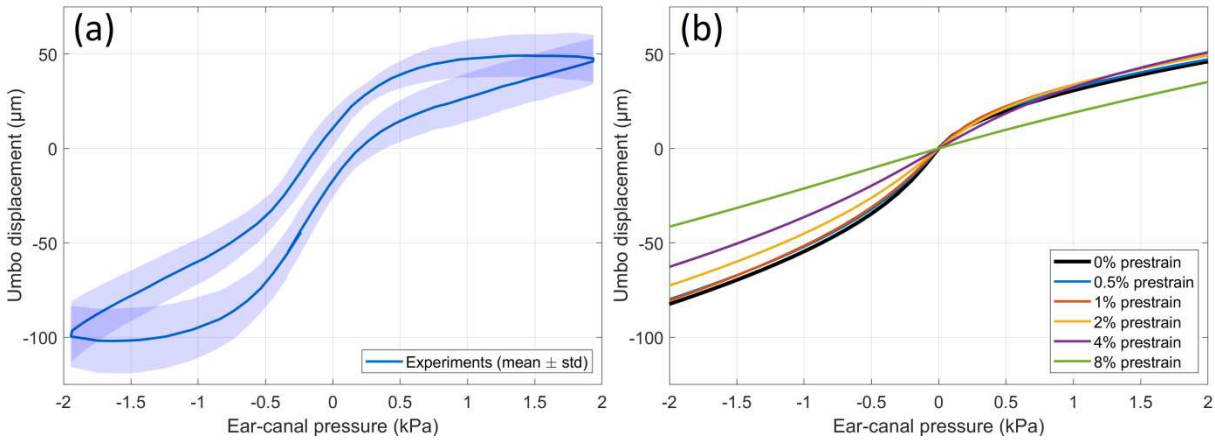


**Fig. 3.** Umbo displacement as a function of static pressure on the tympanic membrane applied at the side of the ear canal. (a) Mean and standard deviation of measured displacement in response to quasi-static pressure cycles in rabbit (Gladiné and Dirckx, 2019). (b) Long-term static displacement in the model for different degrees of prestrain. Positive (resp. negative) displacements denote medial (resp. lateral) displacements. The nonlinearity of the displacement and the asymmetry between positive and negative pressures reduces as the prestrain increases.

## *3.3. Harmonic response*

### *3.3.1. Normal middle-ear response*

Fig. 4 shows the velocity response of the rabbit ME for three experiments measured at the umbo (a) and for the model evaluated at the umbo and footplate with different degrees of prestrain (b). Measurements were obtained on fresh cadaveric rabbit ears using laser Doppler vibrometry. In the experiments, sound pressures were applied at the entrance of the ear canal in a closed acoustic chamber and measured just lateral to the TM. Vibrations were measured from the medial side of the umbo after opening the bulla. Prior to measurement, the TM was maintained hydrated.

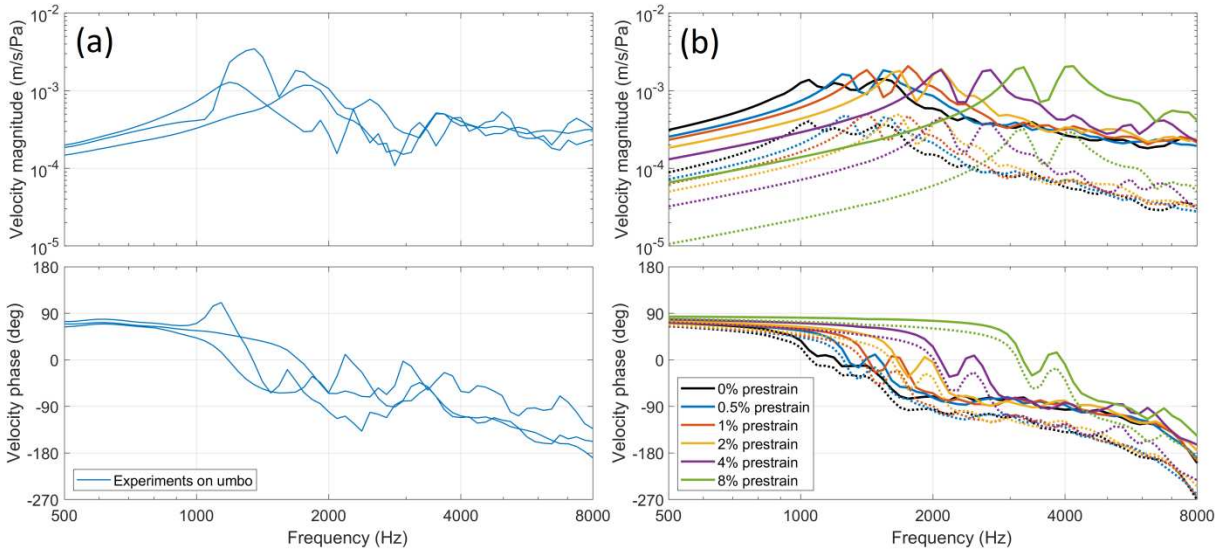


**Fig. 4.** Velocity magnitude (top) and phase (bottom) as a function of frequency in the rabbit ME. (a) Velocity measurements on the umbo on cadaveric rabbit ears. (b) Velocity response of the model for different degrees of prestrain, evaluated at the umbo (solid lines) and footplate (dashed lines). Increasing the prestrain substantially reduces the low-frequency magnitude and shifts the peak frequencies to the right.

In the base model without prestrain, the low-frequency magnitude is higher and the first peak frequency is lower than in the measurements. When the prestrain is increased from 0% to 0.5%, 1%, 2%, 4% and 8%, the low-frequency magnitude at 125 Hz decreases by respectively 1.4, 2.1, 4.0, 6.9 and 12.9 dB, while the peak frequency increases by respectively 228, 374, 623, 1038 and 2143 Hz. The velocity response at high frequencies is affected much less by the prestrain. For prestrains of 0.5%, 1% and 2%, the model shows the best agreement with the measurements. For prestrains of 4% and 8%, the peak frequency and low-frequency magnitude disagree considerably with the experiments, again suggesting that those prestrain levels are too extreme for the current base model. As the prestrain increases from 0% to 0.5%, 1%, 2%, 4% and 8%, we generally observe a small gradual increase of the umbo-to-footplate velocity ratio, with values at 125 Hz ranging from 10.9 dB to 10.9, 11.2, 11.2, 12.0 and 15.8 dB, respectively. In previous experiments in rabbit (Peacock et al. 2015), the average umbo-to-footplate ratio at 125 Hz was equal to 10.2 ± 1.4 dB, leaving only the 4% and 8% prestrain models outside of the experimental standard deviation bounds.

The drop of the magnitude at low frequencies and the shift of the peak frequency in Fig. 4 (b) are phenomena that indicate an increase in stiffness of the structure. Similarly, it can be seen that the first magnitude peak and phase drop in Fig. 4 (b) become slightly sharper as the prestrain increases, which indicates a decrease in damping of the structure. Instead of incorporating prestrain in the TM to simulate the harmonic response of the ME, the traditional approach is to adjust the material parameters until a good match with experimental data is obtained,

310 although this approach is not preferred when the material contains prestrain. If we test this approach by simply doubling the values of all shear moduli, bulk moduli and Young's moduli and halving the loss factors of all structures, then we obtain a frequency response that shows a good agreement with the measurements and is in many aspects similar to the base model with a TM prestrain of 2%, as depicted in Fig. 5.

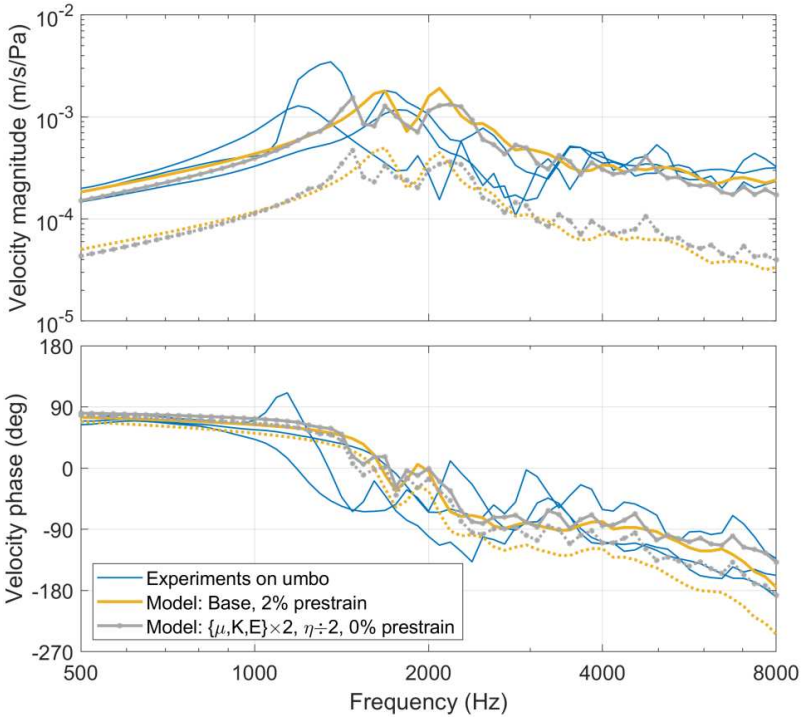


315 **Fig. 5.** Comparison between experimental data, a model with 2% prestrain and a model without prestrain but with adapted material parameters (full lines = umbo, dashed lines = footplate). When prestrain is ignored, a good match with the experiments can be reached by appropriately increasing the elastic moduli and decreasing the damping factors of all components.

### *3.3.2. Middle-ear response with structural changes*

Fig. 6 shows the change in footplate velocity magnitude and phase after creating a 2-mm diameter perforation 320 in the TM for a model with and without prestrain. Prestrain values of 0.5%, 1% and 2% were evaluated, as they were found to be viable prestrain values for the present model in relation to the measurement data, as depicted in Fig. 4. We observe that the velocity magnitude changes relative to the intact case by maximally 10 dB but less than 5 dB on average, both with and without including prestrain. However, when prestrain is included there is a small increase of the velocity ratio of up to 1.5 dB at low frequencies that increases with increasing prestrain. To 325 confirm that the change in the low-frequency response is indeed due to changes in the prestrain after perforation, we also added the result of a model with 0% prestrain but with modified material parameters to match the 2% prestrain model from Fig. 5. We see that the latter model produces the same velocity ratio at low frequencies as the base model with 0% prestrain; hence, prestrain is indeed responsible for the increase in velocity ratio. This

conclusion cannot be drawn at higher frequencies, where differences are largely due to the difference in the absolute model responses of the different prestrain values. When we consider the position of the magnitude peak (not shown), we find that the peak frequency is reduced more in the base model with 2% prestrain (351 Hz) than in the modified model without prestrain (97 Hz) after the perforation is made. Fig. 7 shows the von Mises strain in the PT after creating the perforation. It can be seen that the perforation releases part of the prestrain just inferior and anterior to the location of the hole for all prestrain levels when compared to the normal model (Fig. 2).

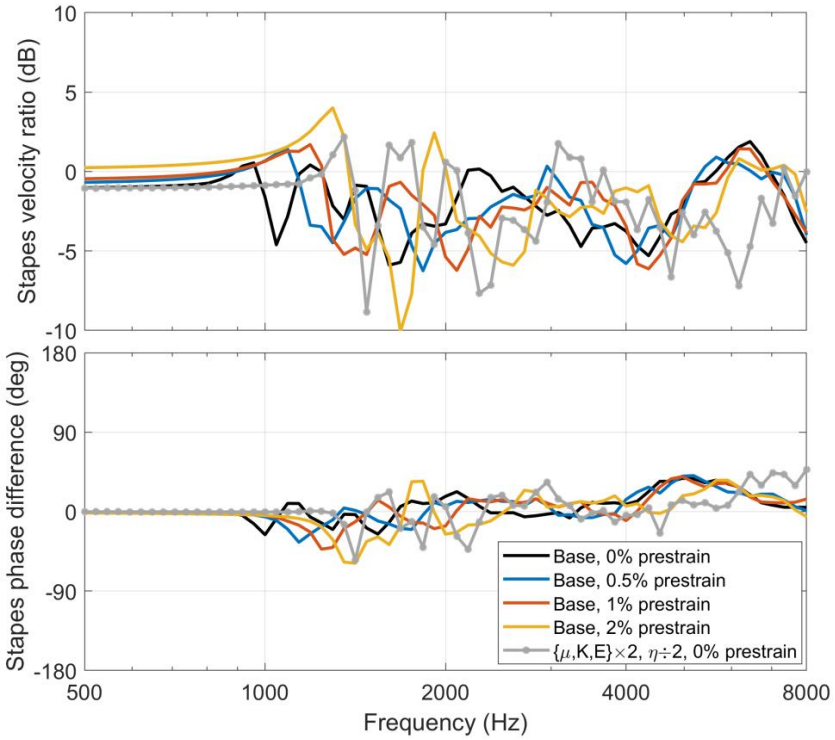


**Fig. 6.** Change in stapes velocity magnitude and phase after creating a 2-mm diameter perforation in the tympanic membrane, both with and without taking prestrain into account. The velocity magnitude changes by less than 5 dB on average for each condition. When prestrain is included, the magnitude ratio at low frequencies increases compared to the model without prestrain.

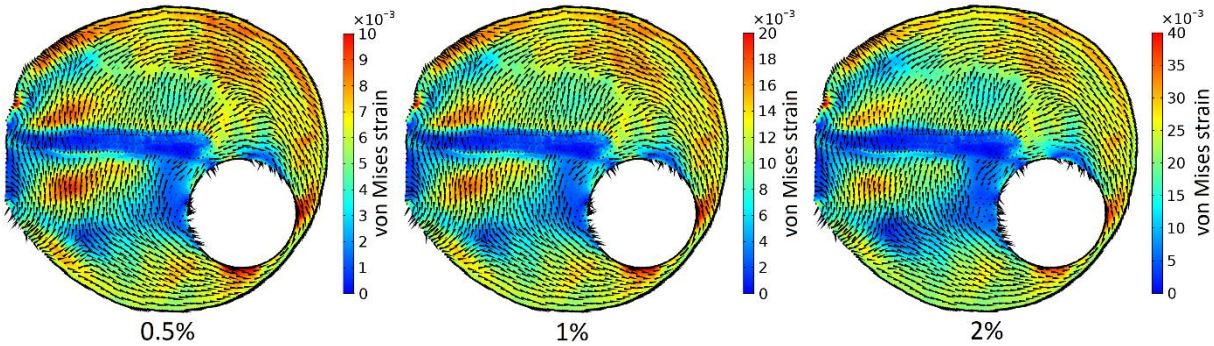


**Fig. 7.** Von Mises strain field and direction of the first principal strain in the pars tensa, after prestraining and perforating the membrane for prestrain levels of 0.5%, 1% and 2%. Creating the perforation partially releases the prestrain just inferior and anterior to the location of the hole.

### *3.4. Sensitivity analysis*

To evaluate how possible uncertainty in the base parameters of Table 1 propagates to the output of the prestrain simulations, we performed a sensitivity analysis in which the base parameters of the model were varied by factors 1/4, 1/2, 2 and 4. For this analysis we focused on the elastic parameters $\mu$, $K$ and $b$ of the PT. In addition, to determine the effect of uncertainty in the remaining ME parameters (the ossicles, joints and ligaments), we simultaneously varied $\mu$, $K$ and $E$ of these components by the same amount. To quantify the model sensitivity to each parameter, we computed the effect on the low-frequency magnitude drop at 125 Hz and the peak frequency shift for a TM prestrain of 2%. The results of the sensitivity analysis are shown in Fig. 8. The results make clear that an increase of the PT elastic parameters leads to a further decrease of the low-frequency magnitude change and a further increase of the peak frequency shift, with the highest effect caused by $\mu$. Hence, the higher the stiffness of the PT, the higher the effect of the prestrain on the harmonic response. For the other ME components, increasing the elastic parameters reduces the drop of the low-frequency magnitude, but increases the peak-frequency shift by a small amount.

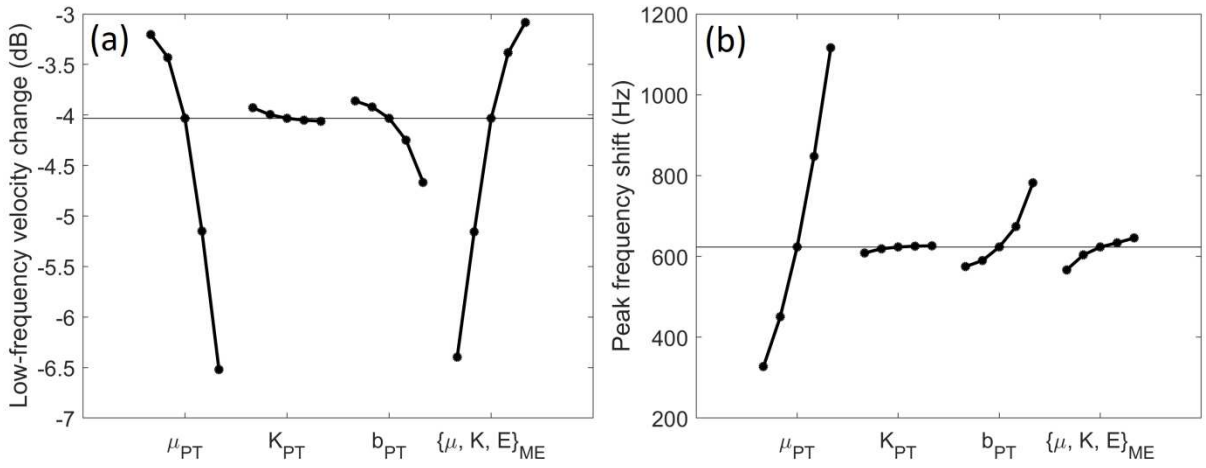


**Fig. 8.** Effect of varying the elastic parameters of the pars tensa (PT) and the other middle-ear (ME) components by factors 1/4, 1/2, 2 and 4 on the low-frequency magnitude change at 125 Hz (a) and the peak frequency shift (b), when the prestrain applied to the pars tensa is 2%.

## 4. Discussion

### *4.1. Comparison to previous work*

#### *4.1.1. Modeling approach to include prestrain*

In the literature, different approaches have been developed to incorporate prestrain and prestress in biomechanical systems. Rausch and Kuhl (2013) simulated prestrain and prestress in the mitral leaflet by stretching the structure from an unstressed initial geometry to a given prestressed reference geometry, assuming that the

deformation gradient induced by the prestress is known. Alternative methods that have been created do not require the existence of an unstressed geometry, because the prestress is incorporated directly in the reference geometry (Alastrue et al., 2007; Maas et al., 2016). Other techniques make use of a reverse engineering approach to seek the deformation gradient that renders the (pre)stresses in equilibrium with the given *in-vivo* loads in the reference geometry (Gee et al., 2010; Weisbecker et al., 2014; Grytz and Downs, 2013; Pierce et al., 2015). To achieve this, an iterative computation scheme is followed due to the nonlinearity associated with large deformations. A similar approach effectively aims to retrieve the unstressed geometry that balances the *in-vivo* loads in the prestressed reference configuration (Bols et al., 2013). The method used in our work is most similar to the latter method, although in our case the *in-vivo* loads are given by prescribed displacements applied to the rim of the TM.

#### *4.1.2. Modeling of prestrain in the tympanic membrane*

To the best of our knowledge, there are only two studies that investigated the effect of prestrain in the TM on the ME vibration response. In Caminos et al. (2018), prestrain was applied directly to the body of the TM as a homogeneous and isotropic strain in the plane of the membrane, while the TM was compressed in transverse direction to account for the Poisson effect. Because their model was based on infinitesimal (linear) deformation theory, they only analyzed the response to small prestrains (0.1–1%). Moreover, because there was no mechanism to eliminate the distortion of the geometry upon prestraining, applying larger strains would have distorted the reference geometry too much, affecting the model results. Their results showed that even small degrees of prestrain had a substantial effect on the TM's modal frequencies. They also found that increasing the prestrain or increasing the Young's modulus had a similar effect on the TM modal frequencies, although both actions led to a different distribution of the modal frequencies in the high-frequency range. Another study investigated the effect of prestrain on the TM response in a model of the locust ear (Malkin et al., 2014). They incorporated prestrain by applying in-plane displacements to the TM which resulted in membrane strains of 1%. The resulting effect on the membrane's time-dependent motion was evaluated in response to pure-tone stimuli of 5, 10, 15, 20 and 25 kHz. Although they made use of linear elasticity theory and had no mechanism to eliminate the geometrical distortion, it was shown that the inclusion of prestrain was needed to explain the presence of flexural waves and the localization of kinetic energy in the membrane.

### *4.2. The effect of prestrain on the harmonic response*

#### *4.2.1. The intact middle ear*

The decrease of the low-frequency magnitude and shift of the peak frequency with increasing prestrain seen in Fig. 4 (b) reflects a similar behavior as an increase of the stiffness of the system, as was deduced by Caminos et

al. (2018) and Malkin et al. (2014). It is well-known that prestress increases the effective stiffness of a mechanical body, which is known as a phenomenon called prestress stiffening. For a harmonic viscoelastic system, prestress introduces an additive term to the global stiffness matrix, called the geometric stiffness matrix (Morman and Nagtegaal, 1983), hence increasing the total stiffness of the structure. In Fig. 4 (b), the first resonance peak in the ME response becomes slightly sharper with increasing prestrain, denoting a decrease of damping in the system. The loss factor, which characterizes the viscoelastic damping in a harmonic system, is defined as the loss modulus over the storage (or elastic) modulus. Because the loss modulus does not increase in the same way as the elastic modulus when the prestress is raised, the effective loss factor will decrease with increasing prestress (Rao et al., 1992; Manconi et al., 2013). Although the approach is not preferable, one may choose to increase the elastic moduli and decrease the loss factors in the base model to replicate the normal ME response instead of incorporating prestrain, as was shown in Fig. 5. However, the adjusted material parameters may not be realistic compared to measurements of material properties on the respective tissue structures (e.g. Cheng et al., 2007; Gan et al., 2011; Zhang and Gan, 2011), which reduces the predictive power of the model beyond the conditions it was validated to. If one does decide to exclude prestrain and wants to verify if the assigned material parameters are in agreement with experimental observations, one should take into consideration whether the experimental data were collected in conditions where the prestrain or prestress was still present or had been eliminated, e.g. by excision of the tissues. In the current rabbit model, soft-tissue elastic parameters were used from measurements obtained in human (Cheng et al., 2007; Gan et al., 2011; Zhang and Gan, 2011). Depending on how the elastic parameters in human are representative for the unknown parameters in rabbit, the results of the model may be affected as illustrated in the sensitivity analysis of Fig. 8, which shows the effect of varying the base parameter values by factors 1/4, 1/2, 2 and 4.

During the generation of the TM prestrain in the model, the ME input geometry is deformed iteratively until all stresses in the system are in equilibrium in the prestressed reference geometry. As a result, a certain degree of prestrain and prestress is built up in the ME components other than the PT. The effect of this can be seen when considering the ratio of the umbo and footplate velocity depicted in Fig. 4 (b), which increases slightly with increasing prestrain. Sensitivity analyses of the ME response (De Greef et al., 2017) have revealed that increasing the stiffness of especially the SAL will reduce the footplate velocity magnitude, leading to a small increase of the umbo-to-footplate velocity ratio. Since our prestrain model also induces a small amount of prestress in the SAL, the observed behavior can be partially explained by an increase of the SAL's effective stiffness. Sim and Puria (2008) presumed that preloads are present in the suspensory ligaments of the ossicles to balance preloads in the

TM and stapes: the pulling force of the TM in the lateral direction associated with the TM prestress may cause a translation and rotation of the IM chain, resulting in prestress of the ligaments. This is also what we observe in our model, where the umbo and ossicles are being pulled outwards as the prestrain is applied to the TM. From a different perspective, the ossicles and their ligaments change their orientation during the neonatal growth process, which may lead to an inward retraction and possibly also a prestraining of the TM while it is growing, hence giving the membrane its inward conical shape (Marcusohn and Dirckx, 2011). Also in simulations of the IM joint, prestrain needed to be incorporated in the joint to obtain a sufficient agreement with measurements of quasi-static motion of the IM complex (Ihrle et al., 2017). The idea that the ossicles, ligaments and joints add to the preservation of prestrain in the TM is supported by the observation that the TM partially loses its shape when the suspensory structures of the ossicles are severed (Dirckx and Decraemer, 2001) or when the manubrium of the malleus is fractured (Gladiné et al., 2018).

#### *4.2.2. The middle ear with structural changes*

To investigate if there are model conditions for which the inclusion of TM prestrain could be important, we created a model with a perforation of 2-mm diameter in the TM and evaluated the change in the ME response after creating the hole, without taking into account the loss of sound pressure gradient across the perforation. We found that the footplate velocity changed by less than 5 dB on average, both when the prestrain was included or not (Fig. 6). However, when prestrain was included there was a small increase of the velocity ratio up to 1.5 dB at low frequencies compared to when prestrain was ignored. In addition, a negative shift of the peak frequency was seen. These findings denote a reduction in the effective stiffness of the TM, which originates from a release in TM prestrain due to the perforation, as observed in Fig. 7. The effect of a TM perforation on the sound-induced footplate response was measured in human by Voss et al. (2001). Despite that they could attribute the observed vibration losses for the most part to a pressure gradient loss across the perforated TM, which was not accounted for in our study, a small difference of up to 5 dB remained after they compensated for the pressure gradient loss, which was ascribed to changes in the structure of the TM and the coupling to the ossicular chain.

Also for other model conditions in which the normal configuration of the TM and ossicles is altered, it can be relevant to include TM prestrain and prestress. Gladiné et al. (2018) simulated the effect of a fracture in the manubrium on the vibration response of the footplate. In their analysis it was necessary to lower the stiffness of the TM to minimize the vibration loss at low frequencies observed in experiments. The lowering of the stiffness was attributed to a presumed loss in TM prestress. By effectively incorporating prestrain and prestress in ME models in future studies, we may improve our insight of ME biomechanics with regard to such phenomena.

## 5. Conclusion

In the present study, a 3D FE model of the rabbit ME was developed to investigate how different levels of prestrain and prestress in the TM affect the ME vibration response. The results reveal a substantial impact on the vibration response of the umbo and stapes footplate: with increasing prestrain, the low-frequency magnitude shows a considerable decrease, while the peak frequency shifts to the higher frequency range. This behavior indicates an increase in stiffness of the material, which is a well-known mechanical phenomenon that occurs when a structure is prestressed. It was shown that the normal ME response can be replicated by appropriately increasing the elastic moduli instead of incorporating prestrain in the model, although this is physically not the preferred approach. TM prestrain may need to be taken into account when the change in ME response is to be investigated due to pathological modifications to the ME structure. This was illustrated by modeling of a ME with perforated TM, which displayed small but noticeable changes in the low-frequency response that result from a release in TM prestrain. In future studies, including such effects may improve understanding of ME mechanics in diseased or reconstructed conditions, which may be relevant for e.g. the development of reconstructive TM tissue grafts.

## Funding

This work was supported by the Research Foundation – Flanders (FWO) [grant number 1211920N].

## CRediT authorship contribution statement

**Pieter Muyshondt:** Methodology, Software, Validation, Formal analysis, Writing – Original Draft, Review & Editing, Visualization, Funding Acquisition. **Joris Dirckx:** Conceptualization, Supervision.

## Declaration of competing interest

The authors declare that they have no known competing financial interests or personal relationships that could have appeared to influence the work reported in this paper.

## Acknowledgements

We acknowledge the Research Foundation – Flanders (FWO) for their financial support, which made this research possible. We thank Dr. Kilian Gladiné for his assistance with the vibration measurements.

## References

Alastrue, V., Pena, E., Martinez, M.A., Doblare, M., 2007. Assessing the use of the "opening angle method" to enforce residual stresses in patient-specific arteries. Ann. Biomed. Eng. 35, 1821–1837. https://doi.org/10.1007/s10439-007-9352-4

Ambrosi, D., Ateshian, G.A., Arruda, E.M., Cowin, S.C., Dumais, J., Goriely, A., Holzapfel, G.A., Humphrey, J.D., Kemkemer, R., Kuhl, E., Olberding, J.E., Taber, L.A., Garikipati, K., 2011. Perspectives on biological growth and remodeling. J. Mech. Phys. Solids 59, 863–883. https://doi.org/10.1016/j.jmps.2010.12.011

Bols, J., Degroote, J., Trachet, B., Verhegghe, B., Segers, P., Vierendeels, J., 2013. A computational method to assess the in vivo stresses and unloaded configuration of patient-specific blood vessels. J. Comput. Appl. Math. 246, 10–17. https://doi.org/10.1016/j.cam.2012.10.034

Buytaert, J.A.N., Salih, W.H.M., Dierick, M., Jacobs, P., Dirckx, J.J.J., 2011. Realistic 3D computer model of the gerbil middle ear, featuring accurate morphology of bone and soft tissue structures. J Assoc Res Otolaryngol 12, 681–696. https://doi.org/10.1007/s10162-011-0281-4

Caminos, L., Garcia-Manrique, J., Lima-Rodriguez, A., Gonzalez-Herrera, A., 2018. Analysis of the mechanical properties of the human tympanic membrane and its influence on the dynamic behaviour of the human hearing system. Appl. Bionics Biomech. 2018, 1–12. https://doi.org/10.1155/2018/1736957

Cescotto, S., Fonder, G., 1979. A finite element approach for large strains of nearly incompressible rubber-like materials. Int. J. Solids Struct. 15, 589–605. https://doi.org/10.1016/0020-7683(79)90073-8

Cheng, T., Dai, C., Gan, R.Z., 2007. Visoelastic properties of human tympanic membrane. Ann. Biomed. Eng. 35, 305–314. https://doi.org/10.1007/s10439-006-9227-0

Chole, R.A., Kodama, K., 1989. Comparative histology of the tympanic membrane and its relationship to cholesteatoma. Ann. Otol. Rhinol Laryngol. 96, 761-766. https://doi.org/10.1177/000348948909801002

De Greef, D., Pires, F., Dirckx, J.J.J., 2017. Effects of model definitions and parameter values in finite element modeling of human middle ear mechanics. Hear. Res. 344, 195–206. https://doi.org/10.1016/j.heares.2016.11.011

Dirckx, J.J.J., Decraemer, W.F., 2001. Effect of middle ear components on eardrum quasi-static deformation. Hear. Res. 157, 124–137. https://doi.org/10.1016/S0378-5955(01)00290-8

Filogamo, G., 1949. Recherches sur la structure de la membrane du tympan chez les différents vertébrés. Cells Tissues Organs 7, 248-272. https://doi.org/10.1159/000140387

Funnell, J., Laszlo, C.A., 1982. A Critical Review of Experimental Observations on Ear-Drum Structure and Function. ORL 44, 181–205. https://doi.org/10.1159/000275593

Gan, R.Z., Yang, F., Zhang, X., Nakmali, D., 2011. Mechanical properties of stapedial annular ligament. Med. Eng. Phys. 33, 330–339. https://doi.org/10.1016/j.medengphy.2010.10.022

Gee, M.W., Forster, C., Wall, W.A., 2010. A computational strategy for prestressing patient-specific biomechanical problems under finite deformation. Int. J. Numer. Methods Biomed. Eng. 26,52–72. https://doi.org/10.1002/cnm.1236

Gladiné, K., Dirckx, J.J.J., 2019. Strain distribution in rabbit eardrums under static pressure. Hear. Res. 381, 107772. https://doi.org/10.1016/j.heares.2019.107772

Gladiné, K., Muyshondt, P., De Greef, D., Dirckx, J., 2018. Effect of malleus handle fracture on middle ear sound transmission: laser Doppler vibrometry measurements and finite element simulations. Proc. 2, 516. https://doi.org/10.3390/ICEM18-05423

Grytz, R., Downs, J.C., 2013. A forward incremental prestressing method with application to inverse parameter estimations and eye-specific simulations of posterior scleral shells. Comput. Methods Biomech. Biomed. Eng. 16,768–780. https://doi.org/10.1080/10255842.2011.641119

Hemilä, S., Nummela, S., Reuter, T., 1995. What middle ear parameters tell about impedance matching and high frequency hearing. Hear. Res. 85, 31–44. https://doi.org/10.1016/0378-5955(95)00031-x

Ihrle, S., Eiber, A., Eberhard, P., 2017. Modeling of the incudo-malleolar joint within a biomechanical model of the human ear. Multibody Syst. Dyn. 39, 291–310. https://doi.org/10.1007/s11044-016-9550-7

Kirikae, I., 1960. The Structure and Function of the Middle Ear. Tokyo University press.

Lim, D.J., 1968. Tympanic membrane part II.: pars flaccida. Acta Otolaryngol. 66, 515–532. https://doi.org/10.3109/00016486809126316

Livens, P., Muyshondt, P.G.G., Dirckx, J.J.J., 2021. Prestrain in the rabbit eardrum measured by digital image correlation and micro-incisions. Hear. Res. 412, 108392. https://doi.org/10.1016/j.heares.2021.108392

Maas, S.A., Erdemir, A., Halloran, J.P., Weiss, J.A., 2016. A general framework for application of prestrain to computational model of biological materials. J. Mech. Behav. Biomed. Mater. 61, 499-510. https://doi.org/10.1016/j.jmbbm.2016.04.012

Maftoon, N., Funnell, W.R.J., Daniel, S.J., Decraemer, W.F., 2015. Finite-element modelling of the response of the gerbil middle ear to sound. JARO 16, 547–567. https://doi.org/10.1007/s10162-015-0531-y

Malkin, R., McDonagh, T.R., Mhatre, N., Scott, T.S., Robert, D., 2014. Energy localization and frequency analysis in the locust ear. J. R. Soc. Interface. 11, 20130857. https://doi.org/10.1098/rsif.2013.0857

Manconi, E., Mace, B.R., Garziera, R., 2013. The loss-factor of pre-stressed laminated curved panels and cylinders using a wave and finite element method. J. Sound. Vib. 332, 1704-1711. https://doi.org/10.1016/j.jsv.2012.09.039

Marcusohn, Y., Dirckx, J.J.J., 2011. Postnatal development of the middle ear in New Zealand white rabbits: ossicles and tympanic ring. Hear. Res. 272, 148-156. https://doi.org/10.1016/j.heares.2010.10.005

Masschaele, B., Dierick, M., Van Loo, D., Boone, M.N., Brabant, L., Pauwels, E., Cnudde, V., Van Hoorebeke, L., 2013. HECTOR: A 240 kV micro-CT setup optimized for research. J. Phys. Conf. Ser. 463, 012012. https://doi.org/10.1088/1742-6596/463/1/012012

Morman, K.N., Nagtegaal, J.C., 1983. Finite element analysis of sinusoidal small-amplitude vibrations in deformed viscoelastic solids. Part I: theoretical development. Int. J. Numer. Methods Eng. 19, 1079–1103. https://doi.org/10.1002/nme.1620190712

Motallebzadeh, H., Charlebois, M., Funnell, W.R.J., 2013. A non-linear viscoelastic model for the tympanic membrane. J. Acoust. Soc. Am. 134, 4427–4434. https://doi.org/10.1121/1.4828831.

Muyshondt, P.G.G., Dirckx, J.J.J., 2021. Structural stiffening in the human middle ear due to static pressure: finite-element analysis of combined static and dynamic middle-ear behavior. Hear. Res. 400, 108116. https://doi.org/10.1016/j.heares.2020.108116

Nelson, D., 2013. Review of methods for determining residual stresses in biological materials, In: Ventura, C.E., Crone, W.C., Furlong, C. (Eds.), Experimental and Applied Mechanics, Volume 4, Conference Proceedings of the Society for Experimental Mechanics Series. Springer New York, New York, NY, pp. 173–182. https://doi.org/10.1007/978-1-4614-4226-4_21

Nelson, D., 2014. Experimental methods for determining residual stresses and strains in various biological structures. Exp. Mech. 54, 695–708. https://doi.org/10.1007/s11340-013-9806-6

O'Connor, K.N., Cai, H., Puria, S., 2017. The effects of varying tympanic-membrane material properties on human middle-ear sound transmission in a three-dimensional finite-element model. J. Acoust. Soc. Am. 142, 2836–2853. https://doi.org/10.1121/1.5008741

Peacock, J., Pintelon, R., Dirckx, J.J.J., 2015. Nonlinear vibration response measured at umbo and stapes in the rabbit middle ear. J. Assoc. Res. Otolaryngol. 16, 569-580. https://doi.org/10.1007/s10162-015-0535-7

Pierce, D.M., Fastl, T.E., Rodriguez-Vila, B., Verbrugghe, P., Fourneau, I., Maleux, G., Herijgers, P., Gomez, E.J., Holzapfel, G.A., 2015. A method for incorporating three-dimensional residual stretches/stresses into patient-specific finite element simulations of arteries. J. Mech. Behav. Biomed. Mater. 47, 147–164. https://doi.org/10.1016/j.jmbbm.2015.03.024

Rao, V.S., Sankar B.V., Sun, C.T., 1992. Constrained layer damping of initially stressed composite beams using finite elements. J. Compos. Mater. 26, 1752-1766. https://doi.org/10.1177/002199839202601204

Rausch, M.K., Kuhl, E., 2013. On the effect of prestrain and residual stress in biological membranes. J. Mech. Phys. Solids 61, 1955-1961. https://doi.org/10.1016/j.jmps.2013.04.005

Sim, J.H., Puria, S., 2008. Soft tissue morphometry of the malleus–incus complex from micro-CT imaging. J. Assoc. Res. Otolaryngol. 9, 5–21. https://doi.org/10.1007/s10162-007-0103-x

Soons, J.A.M., Aernouts, J., Dirckx, J.J.J., 2010. Elasticity modulus of rabbit middle ear ossicles determined by a novel micro-indentation technique. Hear. Res. 263, 33–37. https://doi.org/10.1016/j.heares.2009.10.001

Tian, J., Huang, X., Rao, Z., Ta, N., Xu, L., 2015. Finite element analysis of the effect of actuator coupling conditions on round window stimulation. J. Mech. Med. Biol. 15, 1550048. https://doi.org/10.1142/S0219519415500487

von Békésy, G., 1949. The structure of the middle ear and the hearing of one's own voice by bone conduction. J. Acoust. Soc. Am. 21, 217–232. https://doi.org/10.1121/1.1906501

Voss, S.E., Rosowski, J.J., Merchant, S.N., Peake, W.T., 2001. Middle-ear function with tympanic-membrane perforations. I. Measurements and mechanisms. J. Acoust. Soc. Am. 110, 1432-1444. https://doi.org/10.1121/1.1394195

Weisbecker, H., Pierce, D.M., Holzapfel, G.A., 2014. A generalized prestressing algorithm for finite element simulations of preloaded geometries with application to the aorta. Int. J. Numer. Methods Biomed. Eng. 30, 857–872. https://doi.org/10.1002/cnm.2632

Zhang, X., Gan, R.Z., 2011. Experimental measurement and modeling analysis on mechanical properties of incudostapedial joint. Biomech. Model. Mechanobiol. 10, 713–726. https://doi.org/0.1007/s10237-010-0268-9

585 Zhang, J., Jiao, C., Zou, D., Ta, N., Rao, Z., 2020. Assigning viscoelastic and hyperelastic properties to the middle-ear soft tissues for sound transmission. Biomech. Model. Mechanobiol. 19, 957–970. https://doi.org/10.1007/s10237-019-01263-w